Crystal Structure of Eosinophil Cationic Protein at 2.4 Å Resolution[†,‡]

Ester Boix,[§,||] Demetres D. Leonidas,[§] Zoran Nikolovski,[||] M. Victòria Nogués,[||] Claudi M. Cuchillo,[||] and K. Ravi Acharya*[,§]

Department of Biology and Biochemistry, University of Bath, Claverton Down, Bath BA2 7AY, U.K., and Department de Bioquímica i Biologia Molecular, Facultat de Ciències, Universitat Autònoma de Barcelona, 08193 Bellaterra, Spain

Received August 16, 1999; Revised Manuscript Received October 15, 1999

ABSTRACT: Eosinophil cationic protein (ECP) is located in the matrix of the eosinophil's large specific granule and has marked toxicity for a variety of helminth parasites, hemoflagellates, bacteria, single-stranded RNA virus, and mammalian cells and tissues. It belongs to the bovine pancreatic ribonuclease A (RNase A) family and exhibits ribonucleolytic activity which is about 100-fold lower than that of a related eosinophil ribonuclease, the eosinophil-derived neurotoxin (EDN). The crystal structure of human ECP, determined at 2.4 Å, is similar to that of RNase A and EDN. It reveals that residues Gln-14, His-15, Lys-38, Thr-42, and His-128 at the active site are conserved as in all other RNase A homologues. Nevertheless, evidence for considerable divergence of ECP is also implicit in the structure. Amino acid residues Arg-7, Trp-10, Asn-39, His-64, and His-82 appear to play a key part in the substrate specificity and low catalytic activity of ECP. The structure also shows how the cationic residues are distributed on the surface of the ECP molecule that may have implications for an understanding of the cytotoxicity of this enzyme.

Eosinophils are uniquely endowed with preformed enzymatic and nonenzymatic cationic proteins capable of playing important roles as mediators in the tissue toxicity and inflammation seen in eosinophil-associated allergic, parasitic, neoplastic, and certain idiopathic diseases (*1*). Human eosinophil cationic protein (ECP)[1] and eosinophil-derived neurotoxin (EDN) are major effector proteins located in the eosinophil granule matrix, and their secretion is related to the pathogenesis of inflammatory diseases (*2*, *3*). ECP levels in biological fluids are currently used as an inflammation marker (*4*). Both EDN and ECP produce the neurotoxic Gordon phenomenon in rabbits (*5*). ECP has been characterized in vitro as a potent cytotoxin against a variety of targets, including parasites, bacteria, and mammalian cells, while EDN displays no antibacterial activity and only weak parasitic toxicity when compared to ECP (see ref *3* for a recent review and references therein). Both ECP (also known as RNase-3) and EDN (RNase-2) are ribonucleolytic enzymes and belong to the pancreatic RNase A (EC 3.1.27.5) superfamily. The enzymatic activity of EDN toward most RNA substrates is significantly lower than that of the digestive RNases, and that of ECP is about 100-fold lower still; the in vivo substrates of both enzymes remain to be identified. The ribonucleolytic activity of ECP does not appear to be related to the toxicity against bacteria (*6*). However, both ECP and EDN appear to act as potent neurotoxins utilizing their respective RNase activities (*7*). Moreover, it has been shown recently that ECP and EDN can function in vitro as antiviral agents (*8*, *9*), and ECP degranulation has been correlated with the pathogenesis of respiratory syncytial virus (RSV) bronchiolitis (*10*). The antiviral activity occurs through destruction of isolated virion of the single-stranded RNA respiratory syncytial virus (*8*). These data have generated further interest in understanding the biological functions of eosinophil RNases.

Mature ECP is composed of 133 amino acids (with a signal peptide that is 27 residues long) and is extremely cationic (pI = 10.8) (*11*, *12*). It shares a high degree of sequence identity with EDN (67%) and is 32% identical to RNase A. It possesses the same four disulfide bonds and catalytic triad residues as EDN and RNase A. The divergence rate of ECP from EDN after gene duplication has been calculated to be among the highest of all the primate genes that have been studied (*13*).

In continuing efforts to understand the structure−function relationships of ECP, we have now determined the crystal structure of human recombinant ECP at 2.4 Å resolution. We compare this structure to the high-resolution structures of EDN and RNase A [EDN at 1.83 Å (*14*) and RNase A at 1.2 Å (*15*)] and to the structures of RNase A complexes with the substrate analogues uridine vanadate (*16*), d(CpA) (*17*), and d(ApTpApApG) (*18*). Also, we compare the ECP structure with those of two other members of the RNase family: RNase-4 (a unique member which has a high uridine

[†] This work was supported by MRC (U.K.) Programme Grant 9540039 to K.R.A. and Grants PB96-1172-CO2-01 from the DGES, Ministerio de Educación y Cultura, and 1996SGR-00082 from CIRIT, Generalitat de Catalunya (Spain), to M.V.N. and C.M.C. Thanks are due to Secretaría de Estado de Universidades, Investigación y Desarrollo (Spain), and the Royal Society (U.K.) for a visiting fellowship to E.B.

[‡] The atomic coordinates for ECP have been deposited with the Protein Data Bank (file name 1QMT).

* To whom correspondence should be addressed: Department of Biology and Biochemistry, University of Bath, Claverton Down, Bath BA2 7AY, U.K. Phone: +44-1225-826 238. Fax: +44-1225-826 779. E-mail: K.R.Acharya@bath.ac.uk.

[§] University of Bath.

[||] Universitat Autònoma de Barcelona.

[1] Abbreviations: ECP, eosinophil cationic protein; EDN, eosinophil-derived neurotoxin; RNase A, bovine pancreatic ribonuclease A.

10.1021/bi9919145 CCC: $18.00
Published on Web 12/02/1999

Table 1: X-ray Data Collection and Refinement Statistics

data collection statistics	
space group	hexagonal, $P6_3$ (1 mol/asymmetric unit)
cell dimensions (Å)	$a = b = 100.16$, $c = 31.28$
resolution (Å)	40−2.4
no. of reflections measured	34137
no. of unique reflections	6916
completeness (%)	95.7 (65.0)[a]
$I/\sigma(I)$	10.7 (3.5)[a]
R_{merge}[b] (%)	10.7 (28.7)[a]
refinement statistics	
resolution (Å)	20−2.4
no. of reflections	6907
no. of protein atoms	1102
no. of water molecules	27
R_{cryst}[c] (%)	17.6
R_{free}[d] (%)	22.9
rms deviations from ideality	
bond lengths (Å)	0.010
bond angles (deg)	1.5
dihedrals (deg)	28.1
impropers (deg)	0.8
average *B*-factor (Å^2)	
main chain atoms	36.9
side chain atoms	40.6
water molecules	38.8
all protein atoms	38.8

[a] Outermost shell being 2.49−2.4 Å. [b] $R_{merge} = \Sigma_h\Sigma_i|I_{(h)} - I_{i(h)}|/\Sigma_h\Sigma_i I_{i(h)}$, where $I_{i(h)}$ and $I_{(h)}$ are the ith and mean measurements of the intensity of reflection h. [c] $R_{cryst} = \Sigma_h|F_o - F_c|/\Sigma_h F_o$, where F_o and F_c are the observed and calculated structure factor amplitudes of reflection h, respectively. [d] R_{free} is equal to R_{cryst} for a randomly selected test set of reflections (8%) not used in the refinement.

specificity) (*19*) and angiogenin (RNase-5, a protein that possesses very weak ribonucleolytic activity and is implicated in neovascularization during tumor growth) (*20*, *21*). The structure provides a clearer view of the functionally important regions of the ECP molecule that may shed light on the differences in the catalytic and antipathogenic activities of ECP and EDN.

EXPERIMENTAL PROCEDURES

The recombinant ECP was expressed in *Escherichia coli* and purified as described previously (*22*). Briefly, a synthetic gene for human ECP was cloned into the pET11c expression vector, and the protein was purified from inclusion bodies. The recombinant ECP, which contains an additional formylmethionine residue at the N-terminus, has the same specific activity as the natural protein.

Crystals of ECP were grown at 16 °C by the vapor diffusion hanging drop method. Initial crystallization trials produced needle-shaped crystals after mixing 2 μL of ECP (∼13 mg/mL) with an equal volume of a reservoir solution containing 0.5 M NaCl, 10% 2-propanol, and 0.1 M Hepes buffer at pH 8.0. Microseeding techniques were employed to increase the size of the crystals for X-ray structure analysis. A data set to 2.4 Å resolution was collected on station PX9.5 at Daresbury, U.K., at room temperature using a 30 cm diameter MAR-Research image plate. Processing, scaling, and merging was accomplished with the HKL package (*23*) (Table 1).

The structure of ECP was determined by molecular replacement with the program AMoRe (*24*) using a homology model based on the structure of EDN (*14*). The final model [refined using X-PLOR (*25*)] (between 20 and 2.4 Å) includes 1102 protein atoms and 27 bound water molecules with an R_{cryst} of 17.6% and an R_{free} of 22.9% (Table 1). Analysis of the Ramachandran plot showed that all residues lie in the allowed regions. The entire structure is well-defined except the loop from Asn-87 to Ser-94 and the side chains of Arg-28, Gln-58, Arg-75, Asn-95, Arg-97, and Arg-121, all of which have high temperature factors and are partially disordered.

RESULTS AND DISCUSSION

Overall Structure. The topology of the ECP molecule (∼44 Å × 37 Å × 41 Å) consists of the "RNase A fold" and is closely similar to that of other RNase A homologues (Figure 1A). Least-squares superpositions of ECP with RNase A, EDN, Ang, and RNase-4 (Table 2) indicate that the structure of ECP is most similar to that of EDN, as reflected in pairwise amino acid sequence comparisons (Figure 1B). The regions that deviate most significantly between ECP and EDN involve loop regions (ECP numbering) of residues 17−21 (L2), 33−36 (L3), 88−94 (L6), and 116−119 (L7) (see Figure 1A). Both eosinophil RNases show major differences in their overall structures in two loop regions in comparison with RNase A, Ang, and RNase-4: (a) loop L2 (residues 17−21) separating helices α1 and α2, which is truncated, and (b) loop L7 (residues 115−122) between strands β4 and β5, which contains a large insertion (Figure 1B). As in the EDN structure, loop L7 is packed against the N-terminus, through H-bond interactions. Six water molecules have been identified in the ECP catalytic site (Figure 2); four of these are also present in the RNase A (*15*) and EDN (*14*) structures.

Structural Basis for ECP Substrate Specificity and Low Catalytic Activity. The catalytic site of the RNase A molecule contains several subsites for binding the various phosphate, base, and ribose moieties of the RNA substrate. These sites are designated as $P_0\cdots P_n$, $B_0\cdots B_n$, and $R_0\cdots R_n$, respectively (*26*). The main sites are P_1, at which phosphodiester bond cleavage occurs; B_1, which interacts with the base whose ribose contributes its 3′-oxygen to the scissile phosphodiester bond; and B_2, which binds the base whose ribose provides the 5′-oxygen to the P_1 phosphate. B_1 has nearly absolute specificity for pyrimidines, whereas B_2 strongly prefers purines. This nomenclature will be followed while describing the catalytic and substrate binding sites in ECP.

Previous kinetic analysis indicated that the substrate specificity of ECP resembles that of EDN, with a slight preference for cytosine versus uracil at B_1, and a strong preference for adenine in its B_2 purine binding site (*27*, *28*). The catalytic efficiency of ECP toward all tested substrates is much lower than that of EDN. ECP was found to be most active with tRNA and virus single-stranded RNA (*27*, *29*), and the activity of ECP toward yeast RNA was reported to about 100-fold lower than that of EDN (*29*). Recent kinetic characterization of recombinant ECP for mono-, di-, and polynucleotides showed a distinct cleavage pattern which suggests that ECP acts largely through an exonucleolytic mechanism (*22*). This study of the ECP structure has revealed some details of the active site and substrate interaction subsites.

The positions of catalytic and putative substrate binding residues of ECP have been compared with those of the

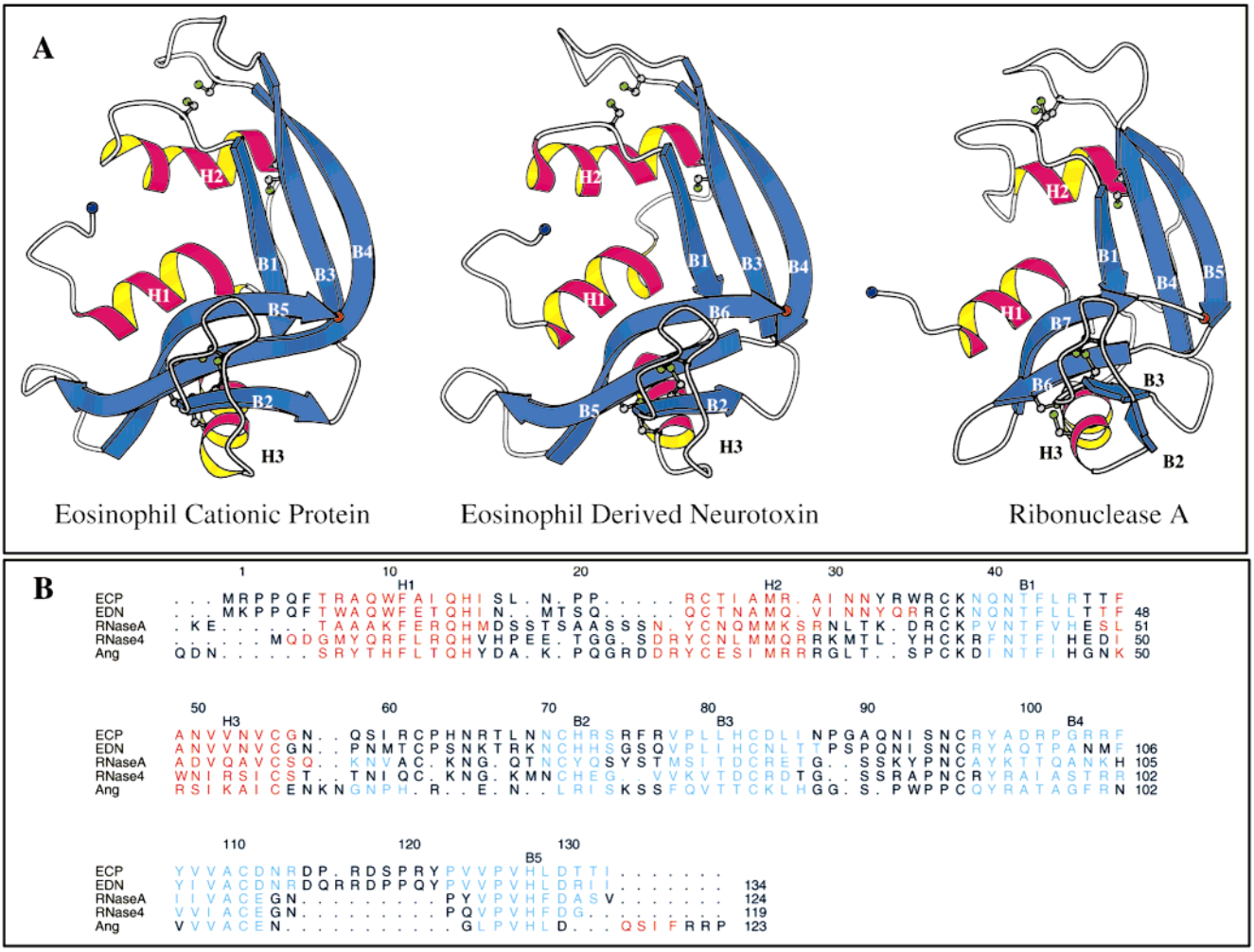

FIGURE 1: (A) Schematic diagram for ECP, EDN, and RNase A. Secondary structure elements were assigned on the basis of the program DSSP (*52*). The secondary structure elements in ECP are helix α1 (Thr-6−Ile-16), strand *β*1 (Asn-39−Arg-45), loop L1 (Met-0−Phe-5), helix α2 (Arg-22−Asn-32), strand *β*2 (Asn-70−Ser-74), loop L2 (Ser-17−Pro-21), helix α3 (Thr-47−Gly-56), strand *β*3 (Val-78−Ile-86), loop L3 (Tyr-33−Lys-38), strand *β*4 (Arg-97−Arg-114), loop L4 (Asn-57−Asn-69), strand *β*5 (Pro-123−Ile-133), loop L5 (Arg-75−Arg-77), loop L6 (Asn-87−Cys-96), and loop L7 (Asp-115−Tyr-122). This figure was created with the program MOLSCRIPT (*53*). (B) Structure-based sequence alignment of ECP, EDN (*14*), RNase A (*15*), RNase-4 (*19*), and Ang (*21*) as determined using the program SHP (*54*). Secondary structural elements (α-helices and *β*-strands) as determined by DSSP (*52*) are also red and blue, respectively. Every tenth residue in the ECP sequence is numbered.

Table 2: Structural Comparison of ECP (RNase-3) with Other RNase A Homologues

RNase A homologue[a]	no. of equivalent residues	root-mean-square deviation (Å)
RNase A	116	1.83
EDN (RNase-2)	132	1.46
RNase-4	112	2.04
Ang (RNase-5)	105	2.43

[a] RNase A [7rsa (*15*)], EDN (*14*), RNase-4 [1rnf (*19*)], and Ang [1b1i (*21*)].

corresponding residues in the structures of phosphate-free RNase A (*15*), the EDN−sulfate complex (*14*), and substrate analogue complexes of RNase A (*16*−*18*) (Figure 3 and Table 3).

P_1 Subsite (Figure 3A). The two histidines (His-12 and His-119) and the lysine (Lys-41) that form the catalytic triad of RNase A are conserved in ECP as His-15, His-128, and Lys-38, respectively. Site-directed mutagenesis of both His-128 to Asp and Lys-38 to Arg has confirmed that these two residues are crucial for the ribonucleolytic activity of ECP (*6*). The orientation of His-15 is almost identical to that of its counterparts in both EDN and RNase A (Figure 3 and Table 3). In ECP, Lys-38 Nζ interacts with Gln-14 Oϵ1, as for the corresponding interactions in EDN and RNase A structures. The orientation of the side chain differs somewhat from that in the other proteins, but it is unclear whether this has any functional significance since Lys-41 of RNase A is known to be quite flexible and to adopt various positions in different structures of free RNase A and RNase A complexes. The four conserved water molecules in the active site of the free ECP structure make extensive H-bond interactions (Figure 2). Among these, one water molecule interacts with both His-15 Nϵ2 and His-128 Nδ1 and occupies the phosphate and sulfate positions as observed in the d(CpA)−RNase A complex and sulfate-bound EDN structures, respectively. Two other water molecules are found at the same position as the O2 atom of the cytosine and the O2P atom of the phosphate in the d(CpA)−RNase A complex. Finally, the fourth water molecule appears to be involved in a main chain interaction with Arg-7 (see Figure 2 and Table 3).

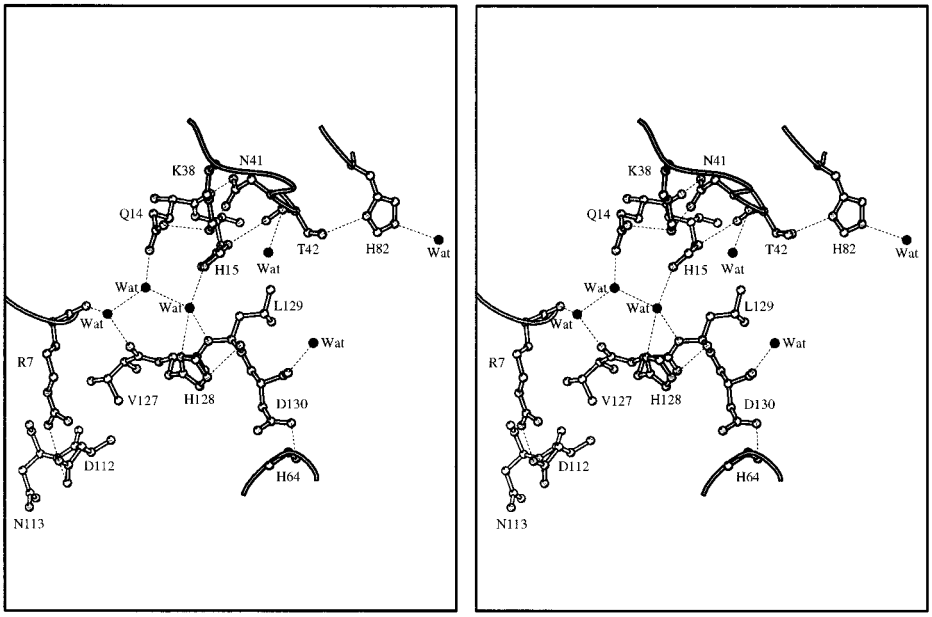

FIGURE 2: Stereodiagram showing the details of the ECP ribonucleolytic active site, including water molecules (in spheres). Broken lines represent hydrogen bonds.

Differences between the interactions of His-128 of ECP and those of His-119 of RNase A may account in part for the reduced catalytic efficiency of ECP. The side chain of His-119 in RNase A has been found to occupy two distinct positions, denoted as A and B (*30*). In position A, the Nϵ2 of His-119 forms a hydrogen bond with Asp-121 Oδ1, and His-119 Nδ1 can then interact with the ligand (*17*). In the sulfate-bound form of the EDN structure (*14*), His-129 adopts the B (inactive) conformation. In the ECP structure, His-128 is in the A (active) conformation, although its position appears to be slightly shifted from that of RNase A. Furthermore, the side chain of Asp-130 adopts a conformation different from its counterpart in RNase A (Asp-121) (Figure 3A) and does not interact with His-128, although it does make a H-bond with the main chain nitrogen of His-64 similar to the Asp-121−Lys-66 H-bond in RNase A. The weakening of the His−Asp interaction in eosinophil RNases has been suggested previously by Sorrentino and Libonati (*28*) to explain the reduction in activity and the lower pH range for optimum activity for the transphosphorylation reaction. The involvement of Asp-121 in a His−Asp catalytic dyad in RNase A was originally suggested by Richards and Wyckoff (*26*) and has been recently studied by site-directed mutagenesis. Schultz et al. (*31*) proposed a major role for Asp-121 in the orientation of the proper tautomer of His-119. Replacing Asp-121 with an Asn or Ala reduced the catalytic efficiency by a factor of about 10- or 100-fold, respectively. In the structures of both Asp-121-Asn and Asp-121-Ala variants of RNase A, His-119 still occupied the A conformation, although its position was slightly shifted, a scenario somewhat similar to that observed in ECP.

B_1 Subsite (Figure 3B). ECP exhibits a similar preference for cytosine over uracil at the B_1 position (*22*) as RNase A (*26*). The position of Thr-42 is equivalent to that of Thr-42 in EDN and Thr-45 in RNase A. The possibility of ambivalent interactions such as those of Asp-83 and Ser-123 in RNase A with Thr-45 and the pyrimidine base through water, which contribute to the flexibility of the B_1 site in interacting with either cytosine or uracil (*17, 32*), cannot be analyzed from the free ECP structure and must await studies on ECP−substrate analogue complexes. Thr-132 in ECP (the counterpart of Ser-123 in RNase A) may participate in interactions similar to those found in RNase A, while Ile-133 in EDN cannot. On the other hand, His-82 in ECP interacts with Thr-42 (Table 3), and might influence the specificity of ECP in the B_1 subsite like Asp-83 in RNase A (*32*, *33*). A similar interaction between His-82 and Thr-42 was observed in the EDN structure, although the side chain of His-82 adopts a somewhat different orientation in EDN and ECP. Finally, Leu-129 may be involved in hydrophobic interactions with the pyrimidine base, like Phe-120 in RNase A. Site-directed mutagenesis on RNase A has shown that Phe-120 participates in the binding of the substrate and in stabilizing the transition state intermediate (*34*). In human Ang, Leu to Phe replacement at this position increases the ribonucleolytic activity on cyclic mononucleotides and dinucleoside phosphates up to 100-fold (*35*).

B_2 Subsite (Figure 3C). The changes in the B_2 site appear to be an important factor in the specificity and reduced catalytic activity of ECP for polynucleotide phosphates (*22*) and can be attributed to the reduced number of interactions [which might also involve steric conflict(s)] at this site. An impaired interaction of the O-5′-nucleoside with the enzyme determines a less effective conformation of the P−O5′ phosphodiester bond, and reduces the catalytic efficiency as described by Steyaert et al. (*36*) and Yakovlev et al. (*37*).

The key B_2 site residues in RNase A are Asn-71 and Glu-111 (*17*, *38*, *39*). The corresponding residues in both ECP and EDN are Asn-70 and Asp-112. While in EDN the Asn-70 side chain may be able to perform equivalent interactions with purine at the B_2 site, the Asn-70 side chain of ECP appears to be ~4.0 Å farther away from the purine pocket than its counterpart in RNase A [based on superposition with the d(CpA)−RNase A complex (*17*)] and is oriented differently. Thus, Asn-70 might not be able to interact with the base (Table 3) unless it shifted considerably (conformational change) upon ligand binding or participated in a water-mediated interaction. This different positioning is partly due

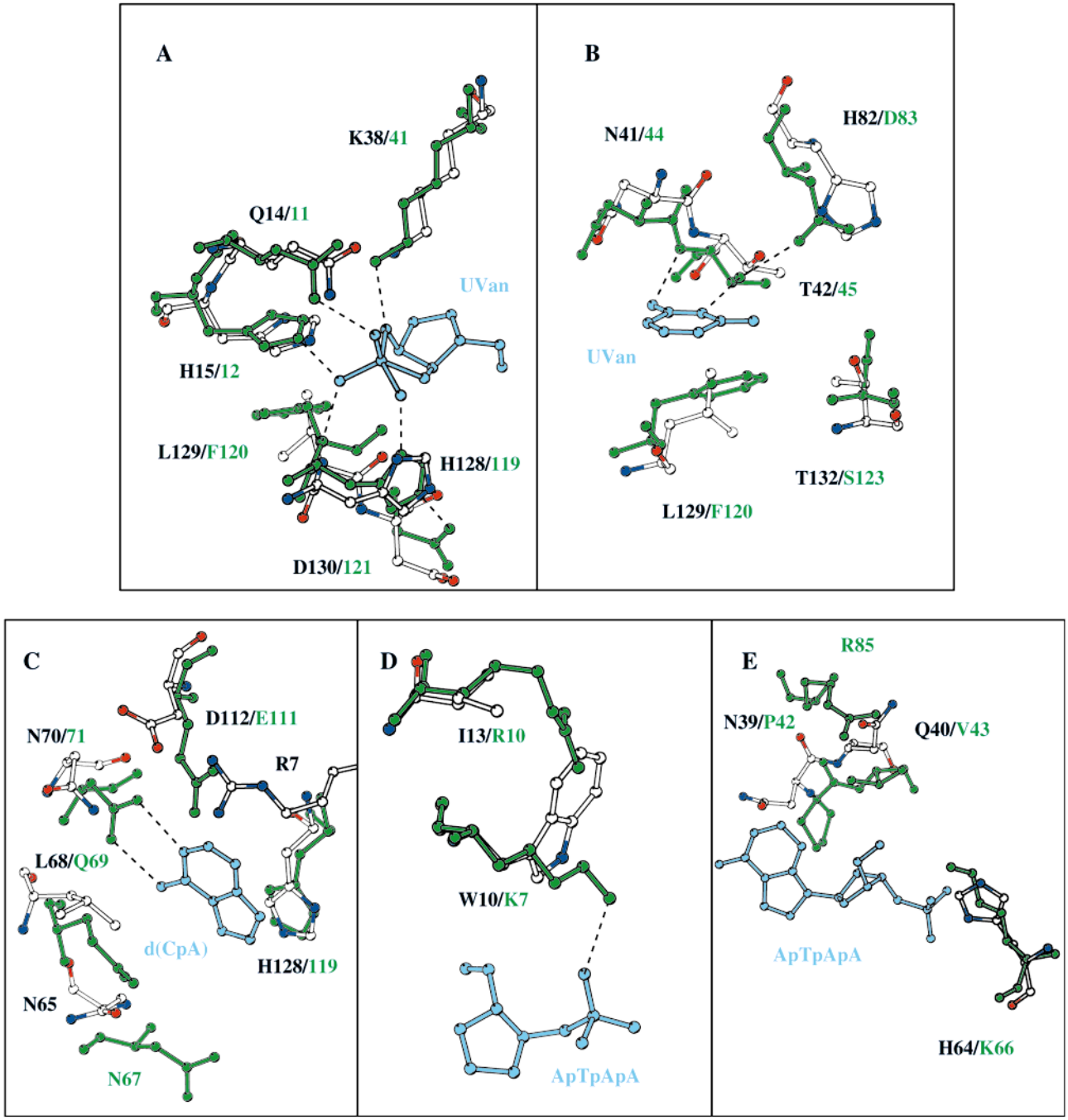

FIGURE 3: (A−E) Superimposed structures of ECP and RNase A−substrate complexes [UVan (*16*), d(CpA) (*17*), and d(ApTpApA) (*18*)] showing subsites P_1 (A), B_1 (B), B_2 (C), P_2 (D), and $B_0/P_0/P_{-1}$ (E). Portions of the substrate analogue molecules are shown (cyan). ECP and RNase A residues are shown in the standard colors and in green, respectively. Broken lines represent hydrogen bonds in the RNase A complex.

to changes in the backbone conformation of the loop of residues 57−69 (ECP numbering). The shorter side chain of Asp-112, as in EDN, cannot mimic the potential interaction of Glu-111 Oϵ2 with the adenine in RNase A. On the basis of mutagenesis results on RNase A, it has been described that Glu-111 is a key residue for interaction with substrates with guanine at the B_2 position (*39*). Interestingly, examination of the ECP structure revealed that Arg-7 (Ala-4 in RNase A and C-mannosylated Trp-7 in authentic EDN) might be a key residue responsible for the base specificity at the B_2 site. In the modeled ECP−d(CpA) complex, the guanidino group of Arg-7 occupies a position similar to that of Glu-111 in the RNase A complex and is about 3.5 Å away from the N3 atom of adenine, suggesting that it might form a H-bond upon complex formation. However, when a guanine is modeled in B_2, the Arg-7 Nη2 atom is 2.2 Å away from the N2 atom of the base (with which it cannot form a H-bond), and this raises the possibility that Arg-7 might hinder guanine binding. This structural observation might explain the extremely low activity of ECP toward UpG as compared to UpA (*22*).

P_2 Subsite (Figure 3D). Kinetic, site-directed mutagenesis and structural studies (*18*, *40*, *41*) have shown that Lys-7 of RNase A is a component of the P_2 site. Lys-7 is substituted by a Trp in the ECP and EDN structures. The Trp in both EDN and ECP appears to be too far from the P_2 phosphate

Table 3: Comparison of Residues in the Catalytic and Substrate Binding Sites of RNase A, ECP, and EDN

	RNase A residue	proposed role(s) in RNase A[a–d]	ECP residue	comments based on the ECP structure (comparison with EDN[e])
P_1	His-12	acts as a base in the transphosphorylation step	His-15	similar position (equivalent in EDN)
		H-bond to phosphate and Thr-45 C═O		H-bond to a water and to Thr-42 C═O
	Lys-41	stabilizes the intermediate in the transition state	Lys-38	
		H-bond to Asn-44, Gln-11, and the 2′-OH		H-bond to Asn-41 and Gln14 (equivalent in EDN)
	His-119	acts as an acid in the transphosphorylation step	His-128	side chain in the active (A) conformation
		H-bond to the O5′ leaving group and the phosphate		H-bond to a water (in EDN, His-129 is in the B form)
		H-bond to the Asp-121 side chain		H-bond to Leu-129 C═O; does not interact with Asp-130
	Gln-11	H-bond to phosphate and to Lys-41	Gln-14	H-bond to a water and to Lys-38 (equivalent in EDN)
B_1	Thr-45	interacts with pyrimidine	Thr-42	can interact with pyrimidine
		H-bond to N3 and O2 of the cytosine		H-bond to His-82 Nδ1 (equivalent in EDN)
	Asp-83	involved in uracil/cytosine specificity	His-82	H-bond to a water and to Thr-42 Oγ1 (similar in EDN)
	Ser-123	water-mediated interaction with cytosine	Thr-132	might make similar interactions (in EDN, Ile-133 cannot)
	Phe-120	stacking interactions with the pyrimidine base	Leu-129	can also be involved in hydrophobic interactions
B_2	Asn-71	interaction with the purine base	Asn-70	cannot interact with the purine (in EDN, like RNase A)
	Glu-111	interaction with the purine base	Asp-112	no possible interaction with the purine (similar in EDN)
			Arg-7	can interact with adenine, but will hinder guanine binding; Arg-7 C═O H-bond to a water (Trp-7 in EDN)
	His-119	stacking interaction with adenine	His-128	equivalent position (in EDN, His-129 is in the B form)
P_2	Lys-7	interaction with phosphate	Trp-10	no interaction (same for Trp-10 in EDN)
P_0	Lys-66	weak interaction with phosphate	His-64	possible interaction with phosphate (in EDN, Arg-132 is in a similar position)
B_0			Asn-39	can interact with a purine base in ECP and EDN
P_{-1}	Arg-85	weak interaction with phosphate	Gln-40	can interact with phosphate (different orientation in EDN)

[a] Phosphate free RNase A [7rsa (*15*)]. [b] Uridine vanadate−RNase A complex [1ruv (*16*)]. [c] d(CpA)−RNase A complex [1rpg (*17*)]. [d] d(ApTpApApG)−RNase A complex [1rcn (*18*)]. [e] Sulfate-bound EDN (*14*). H-bond, hydrogen bond interaction.

for its Nε1 atom to H-bond, and there is no other residue that could perform this role. In addition, the other P_2 site residue in RNase A (Arg-10), which seems to form purely Coulombic interactions with the P_2 phosphate (*41*), is replaced with Ile-13 in ECP and Thr-13 in EDN. The absence of an anchoring site on the 3′-side of the scissile bond may be an additional factor reducing the catalytic efficiency of the enzyme. In RNase A, the P_2 site residues seem to contribute to catalytic efficiency even for short substrates lacking a P_2 phosphate (*40*), most likely by influencing the effectiveness of the active site residues [reducing the pK_a values of the catalytic histidines through Coulombic effects (*42*)]. These observations suggest yet another way in which the alteration of the P_2 site in ECP might have far-reaching effects on potency.

P_0 Subsite (Figure 3E). In the RNase A molecule, Lys-66 was described as part of the P_0 site, although the contribution of this additional site in RNA substrate binding is rather weak compared to that of the P_2 site (*41*, *43*). The position of the Nζ atom of Lys-66 is ∼5 Å away from the phosphoryl group oxygen atom corresponding to the P_0 phosphate in the RNase A−d(ApTpApApG) complex (*18*), and it has been proposed that the contribution is by Coulombic interactions (*41*). Superposition of the ECP structure with that of the RNase A−d(ApTpApApG) complex suggests that His-64 in ECP could contribute to substrate binding at P_0 through similar interactions as in the case of Lys-66 in RNase A since both residues are located at structurally equivalent positions (Table 3). Residue His-64 is unique to the sequences of ECPs from humans and the higher primates. Arg-132 in EDN (Thr-131 in ECP) was suggested to perform a role equivalent to that of Lys-66 in RNase A (*44*). Furthermore, Rosenberg and Dyer (*45*) observed a 10-fold reduction in the catalytic activity of EDN by mutating Arg-132. Superposition of the ECP and EDN structures reveals that the Nη1 atom of Arg-132 from EDN is located about 1 Å from the Nε2 atom of His-64 in ECP (the structurally equivalent residue in EDN is Ser-64).

B_0/P_{-1} Subsite (Figure 3E). The digestion pattern of ECP for polynucleotides, poly(C) and poly(U), was proposed to be determined by an exonuclease-like mechanism (*22*) and could be explained by the reduced level of interaction at the P_2 site and the presence of a strong, new interacting site located upstream at the 5′-side of the P−O5′ cleavable phosphodiester bond. Analysis of the EDN sulfate-bound structure revealed that the position of a secondary sulfate (position B) could mimic a new substrate binding region consisting of residues Arg-36, Asn-39, and Gln-40 in EDN (*14*). The structurally equivalent residues in ECP are Arg-34, Asn-39, and Gln-40. Both Arg-34 and Asn-39 occupy positions almost identical to those of their EDN counterparts. The side chains of Asn-39 in ECP and EDN are at H-bond distance from the B_0 adenine in the d(ApTpApApG)−RNase A complex (*18*). In contrast, the side chains of Gln-40 in ECP and EDN adopt different conformations, pointing in opposite directions. However, it should be noted that Gln-40 in EDN makes an interaction with a sulfate ion from the crystallization medium. Gln-40 in sulfate-free EDN might adopt a conformation similar to that seen in ECP.

The identification of residues in the P_{-1} site in ECP is less clear, as the full characterization of this site in RNase A is not yet available. Recently, Fisher et al. (*46*), on the basis of their kinetic and mutagenesis studies, have described Arg-85 of RNase A as part of the P_{-1} site. Superposition of the ECP and RNase A structures reveals that the side chain of Gln-40 (ECP) is close to that of Arg-85 in RNase A.

Comparison with RNase-4 and Ang Active Site Architecture. Differential arrangements at the catalytic site (mainly B_1) have been analyzed for both RNase-4 and Ang in comparison with ECP. The uridine specificity of RNase-4 at the B_1 site has been mainly explained by the positioning of Phe-42 and Arg-101 (RNase-4 numbering) in the pyrim-

idine pocket (*19*, *47*). The structurally equivalent residues, Gln-40 and Arg-105 in ECP, are located on the surface and cannot participate in base recognition. In the case of Ang, it has been established that the pyrimidine binding site differs significantly in conformation from RNase A and is obstructed by the C-terminal segment even though the catalytic triad is present (*21*). It has been suggested that movement of the entire 3_{10}-helix at the C-terminus would be required for substrate binding to Ang. These features are unique to the Ang structure, and there are no structural similarities in the ECP molecule. Thus, every member of the RNase A family studied so far appears to have different approaches for catalysis and substrate recognition that constitute a key part of its mechanism of action.

Possible Structural Basis for ECP Cytotoxicity. The biological properties of ECP suggest a physiological role in the host defense mechanism. ECP is cytotoxic to bacteria, helminths (*2*), and single-stranded RNA respiratory syncytial virus (*8*). The RNase activity of ECP is necessary for neurotoxicity and antiviral activity (*7*, *8*). However, bactericidal activity is not dependent on the catalytic activity (*6*), and helminthotoxicity is not inhibited by the ribonuclease inhibitor, a 50 kDa leucine-rich protein (*3*).

The antibacterial function of ECP is not shared by EDN or the ECP/EDN precursor and appears to have been generated after gene duplication some 30 million years ago (*48*, *49*). During the process of evolution, after its divergence from EDN, 12 additional arginines of a total of 29 substitutions were incorporated in the ECP gene of the old world primates, leading to a change in the p*I* from 8.4 to 10.6 in a relatively short period of time (*48*). The capacity of ECP to disrupt cell membranes (*50*), the inhibition of in vitro lytic activity on parasites by heparin (*2*), and the correlation between the increase in p*I* and the cytotoxicity suggest that the specific cytotoxicity of ECP appears to be mainly related to the increase in the number of arginine residues in its sequence.

The location of positively charged residues on the ECP molecule has been analyzed. The overall surface charge [calculated using the program GRASP (*51*)] for ECP is 14, while for EDN and RNase A, it is 7 and 3, respectively. All the arginine residues are solvent-exposed, and some are involved in crystal packing. The distribution of the positive charges which are distributed throughout on the surface of ECP molecule does not correspond to that of the basic residues in RNase A that align RNA substrates through electrostatic interactions with the phosphate groups (*43*). In fact, many of the cationic groups in ECP are located far away from the active site cleft. EDN also lacks the extended cationic binding site of RNase A. This differential distribution of surface positive charges in eosinophil RNases was suggested to be related to their inactivity toward double-stranded RNA degradation and their inability to unwind DNA (*28*).

CONCLUSION

Analysis of the ECP structure has contributed to the understanding of ECP's substrate specificity and reduced catalytic efficiency. Numerous substrate analogue and inhibitor complexes have been used to define the detailed architecture of the catalytic site of RNase A. However, a more substantial structure−function analysis, probing the ribonucleolytic active site, will be required to identify the differences in specificity among RNase A homologues. The three-dimensional structure for the unliganded ECP presented here has provided only the first glimpse of the molecule and has provided answers for some of the questions raised by previous kinetic and protein engineering studies. The observed differences in the ECP subsite structure can also account for the favored exonuclease-type mechanism and its failure to accommodate a guanine in B_2. It has also set a sound basis for future studies on ECP−substrate−inhibitor complexes. Such complexes should prove useful in the rational design of inhibitors for ECP and its homologues. Analysis of the epitopes on the ECP molecule may also lead to the identification of new binding sites in the molecule that could explain its cytotoxic properties unrelated to the ribonucleolytic activity.

ACKNOWLEDGMENT

We dedicate this article to Lord Phillips of Ellesmere (David C. Phillips). We thank Dr. R. Shapiro for the constructive criticisms of the manuscript, the staff at the Synchrotron radiation source at Daresbury (U.K.), Drs. A. C. Papageorgiou and J. Swaminathan and Ms. E. Chrysina for their help with X-ray data collection, Drs. S. C. Mosimann and M. N. G. James for the coordinates of EDN, and Drs. S. S. Terzyan and M. Coll for the coordinates of RNase-4.

REFERENCES

1. Gleich, G. J., Adolphson, C. R., and Leiferman, K. M. (1993) *Annu. Rev. Med. 44*, 85−101.
2. Ackerman, S. J. (1993) in *Eosinophils: Biological and Clinical Aspects* (Makino, S., and Fukuda, T., Eds.) pp 33−74, CRC.
3. Snyder, M. R., and Gleich, G. J. (1997) in *Ribonucleases: Structures and Functions* (D'Alessio, G., and Riordan, J. F., Eds.) pp 425−444, Academic Press, New York.
4. Venge, P., and Bystrom, J. (1998) *Int. J. Biochem. Cell Biol. 30*, 433−437.
5. Fredens, K., Dahl, R., and Venge, P. (1982) *J. Allergy Clin. Immunol. 70*, 361−366.
6. Rosenberg, H. F. (1995) *J. Biol. Chem. 270*, 7876−7881.
7. Sorrentino, S., Glitz, D. G., Hamann, K. J., Loegering, D. A., Checkel, J. A., and Gleich, G. J. (1992) *J. Biol. Chem. 267*, 14859−14865.
8. Domachowske, J. B., Dyer, K. D., Adams, A. G., Leto, T. L., and Rosenberg, H. F. (1998) *Nucleic Acids Res. 26*, 3358−3363.
9. Domachowske, J. B., Dyer, K. D., Bonville, C. A., and Rosenberg, H. F. (1998) *J. Infect. Dis. 177*, 1458−1464.
10. Harrison, A. M., Bonville, C. A., Rosenberg, H. F., and Domachowske, J. B. (1999) *Am. J. Respir. Crit. Care Med. 159*, 1918−1924.
11. Barker, R. L., Loegering, D. A., Ten, R. M., Hamann, K. J., Pease, L. R., and Gleich, G. J. (1989) *J. Immunol. 143*, 952−955.
12. Rosenberg, H. F., Ackerman, S. J., and Tenen, D. G. (1989) *J. Exp. Med. 170*, 163−176.
13. Rosenberg, H. F., Dyer, K. D., Tiffany, H. L., and Gonzalez, M. (1995) *Nat. Genet. 10*, 219−223.
14. Mosimann, S. C., Newton, D. L., Youle, R. J., and James, M. N. G. (1996) *J. Mol. Biol. 260*, 540−552.
15. Wlodawer, A., Svensson, L. A., Sjolin, L., and Gilliland, G. L. (1988) *Biochemistry 27*, 2705−2717.
16. Ladner, J. E., Wladkoswki, B. D., Svensson, L. A., Sjolin, L., and Gilliland, G. L. (1997) *Acta Crystallogr. D53*, 290−301.

17. Zegers, I., Maes, D., Dao-Thi, M.-H., Poortmans, F., Palmer, R., and Wyns, L. (1994) *Protein Sci. 31*, 2322−2339.
18. Fontecilla-Camps, J. C., de Llorens, R., le Du, M. H., and Cuchillo, C. M. (1994) *J. Biol. Chem. 269*, 21526−21531.
19. Terzyan, S. S., Peracaula, R., deLlorens, R., Tsushima, Y., Yamada, H., Seno, M., Gomis-Ruth, F. X., and Coll, M. (1999) *J. Mol. Biol. 285*, 205−214.
20. Acharya, K. R., Shapiro, R., Allen, S. C., Riordan, J. F., and Vallee, B. L. (1994) *Proc. Natl. Acad. Sci. U.S.A. 91*, 2915−2919.
21. Leonidas, D. D., Shapiro, R., Allen, S. C., Subbarao, G. V., Veluraja, K., and Acharya, K. R. (1999) *J. Mol. Biol. 285*, 1209−1233.
22. Boix, E., Nikolovski, Z., Moiseyev, G. P., Rosenberg, H. F., Cuchillo, C. M., and Nogués, M. V. (1999) *J. Biol. Chem. 274*, 15605−15614.
23. Otwinowski, Z., and Minor, W. (1997) in *Methods in Enzymology* (Carter, C. W. J., and Sweet, R. M., Eds.) pp 307−326, Academic Press, New York.
24. Navaza, J. (1994) *Acta Crystallogr. A50*, 157−163.
25. Brünger, A. T., and Rice, L. M. (1997) *Methods Enzymol. 277*, 243−269.
26. Richards, F. M., and Wyckoff, H. W. (1971) *Enzymes (3rd Ed.) 4*, 647−806.
27. Sorrentino, S., and Glitz, D. G. (1991) *FEBS Lett. 288*, 23−26.
28. Sorrentino, S., and Libonati, M. (1994) *Arch. Biochem. Biophys. 312*, 340−348.
29. Slifman, N. R., Leogering, D. A., McKean, D. J., and Gleich, G. J. (1986) *J. Immunol. 137*, 2913−2917.
30. Borkakoti, N., Moss, D. A., and Palmer, R. A. (1982) *Acta Crystallogr. B38*, 2210−2217.
31. Schultz, L. W., Quirk, D. J., and Raines, R. T. (1998) *Biochemistry 37*, 8886−8898.
32. Gilliland, G. L., Dill, J., Pechik, I., Svensson, L. A., and Sjolin, L. (1994) *Protein Pept. Lett. 1*, 60−65.
33. delCardayre, S. B., and Raines, R. T. (1995) *J. Mol. Biol. 252*, 328−336.
34. Tanimizu, N., Ueno, H., and Hayashi, R. (1998) *J. Biochem. (Tokyo) 124*, 410−416.
35. Harper, J. W., Auld, D. S., Riordan, J. F., and Vallee, B. L. (1988) *Biochemistry 27*, 219−226.
36. Steyaert, J., Haikal, A. F., and Wyns, L. (1994) *Proteins: Struct., Funct., Genet. 18*, 318−323.
37. Yakovlev, G. I., Bocharov, A. L., Moiseyev, G. P., and Mikhaylov, S. N. (1985) *FEBS Lett. 179*, 217−220.
38. Wodak, S. Y., Liu, M. Y., and Wyckoff, H. W. (1977) *J. Mol. Biol. 116*, 855−875.
39. Tarragona-Fiol, A., Eggelte, H. J., Harbron, S., Sanchez, E., Taylorson, C. J., Ward, J. M., and Rabin, B. R. (1993) *Protein Eng. 6*, 901−906.
40. Boix, E., Nogues, M. V., Schein, C. H., Benner, S. A., and Cuchillo, C. M. (1994) *J. Biol. Chem. 269*, 2529−2534.
41. Fisher, B. M., Ha, J. H., and Raines, R. T. (1998) *Biochemistry 37*, 12121−12132.
42. Fisher, B. M., Schultz, L. W., and Raines, R. T. (1998) *Biochemistry 37*, 17386−17401.
43. Nogués, M. V., Moussaoui, M., Boix, E., Vilanova, M., Ribo, M., and Cuchillo, C. M. (1998) *Cell. Mol. Life Sci. 54*, 766−774.
44. Beintema, J. J. (1989) *FEBS Lett. 254*, 1−4.
45. Rosenberg, H. F., and Dyer, K. D. (1997) *Nucleic Acids Res. 25*, 3532−3536.
46. Fisher, B. M., Grilley, J. E., and Raines, R. T. (1998) *J. Biol. Chem. 273*, 34134−34138.
47. Hofsteenge, J., Moldow, C., Vicentini, A. M., Zelenko, O., Jarai-Kote, Z., and Neumann, U. (1998) *Biochemistry 37*, 9250−9257.
48. Zhang, J. Z., Rosenberg, H. F., and Nei, M. (1998) *Proc. Natl. Acad. Sci. U.S.A. 95*, 3708−3713.
49. Rosenberg, H. F., and Dyer, K. D. (1995) *J. Biol. Chem. 270*, 21539−21544.
50. Young, J. D., Peterson, C. G. B., Venge, P., and Cohn, Z. A. (1986) *Nature 321*, 613−616.
51. Nicholls, A., and Honig, B. (1991) *J. Comput. Chem. 12*, 435−445.
52. Kabsch, W., and Sanders, C. (1983) *Biopolymers 22*, 2577−2637.
53. Kraulis, P. J. (1991) *J. Appl. Crystallogr. 24*, 946−950.
54. Stuart, D. I., Levine, M., Muirhead, H., and Stammers, D. K. (1979) *J. Mol. Biol. 134*, 109−142.

BI9919145